Supplementary Material

TABLE OF CONTENTS

A METRIC-BASED EVALUATION

A.1 EVALUATION METRICS

We evaluate our method along two primary axes: (1) the *semantic integrity* of textual content, and (2) the *perceptual quality* of the reconstructed images. Accordingly, we organize the metrics into two groups.

OCR Metrics. To assess text restoration performance, we report:

- ***F_1* score**, **Precision**, **Recall** and **Accuracy** (↑), : character-level measures of OCR correctness; higher is better.
- **Normalized Edit Distance (1-NED)** (↑): inverse of edit distance, scaled to [0, 100]; higher values indicate closer agreement with the ground truth.

Image-Quality Metrics. For perceptual fidelity, we adopt:

- **Peak Signal-to-Noise Ratio (PSNR)** (↑): log-scaled pixel-level similarity to the reference image.
- **Structural Similarity Index (SSIM)** (↑): evaluates luminance, contrast, and structural consistency in line with human perception, scaled to 0–100.
- **Learned Perceptual Image Patch Similarity (LPIPS Zhang et al. (2018a))** (↓): deep-feature distance reflecting perceptual differences, scaled to 0–100.
- **Multi-Dimension Attention Network for No-Reference IQA (MANIQA Yang et al. (2022))** (↑): no-reference quality score based on attention-driven features, scaled to 0–100.
- **CLIP-based Image Quality Assessment (CLIP-IQA Wang et al. (2023))** (↑): semantic fidelity metric leveraging CLIP embeddings, scaled to 0–100.
- **Multi-Scale Image Quality Transformer (MUSIQ Ke et al. (2021))** (↑): transformer-based no-reference IQA that aggregates multi-resolution cues.

A.2 MISALIGNMENT BETWEEN METRICS AND HUMAN PERCEPTION

SR papers still default to **PSNR**, **SSIM**, and **LPIPS**. Although convenient, these scores often drift from what people actually perceive—especially when the low-resolution input is heavily degraded. Fig. 7 offers four counter-examples that highlight three recurring failure modes.

Perceptual vs. Semantic Fidelity. In Figure 7, the "`HOMER BREWING COMPANY`" sign is reconstructed cleanly by GLYPH-SR yet receives lower PSNR and SSIM than Real-ESRGAN, whose output contains aliasing and hallucinated glyphs.

Metrics Can Be Misleading. Across multiple benchmarks we frequently observe visually superior outputs that score lower on PSNR/SSIM/LPIPS (see red vs. blue values in Figure 7). This misalignment—echoed by prior studies Blau & Michaeli (2018); Jinjin et al. (2020); Gu et al. (2022); Yu et al. (2024a)—underscores the danger of metric-only evaluation. For text-aware SR, side-by-side inspection or user studies remain indispensable.

Figure 7: Each triplet shows (left) the input LR image, (middle) a strong baseline, and (right) GLYPH-SR. Despite GLYPH-SR producing visibly sharper text, its PSNR/SSIM/LPIPS scores (blue) are often lower than those of the baseline (red). The gap exposes a growing consensus: traditional metrics alone do not capture human perception of text-laden imagery.

B EXPERIMENT DETAILS

B.1 REPRODUCIBILITY STATEMENT

Synth Dataset:
https://drive.google.com/drive/folders/1eYMvZQq-93okI2v1YldXLPHDycBkuvdu?usp=drive_link

Pretrained Model:
https://drive.google.com/drive/folders/1hrZ5jRbVLcRSFpbL-uPxe9iLddylAFgk?usp=drive_link

Code:
https://drive.google.com/drive/folders/1A75nhOQEG1hcEhzUJxO75X8LfTO7lR3K?usp=drive_link

Results:
https://drive.google.com/drive/folders/1CArNuM0AI50z3TGsR66u218RLV5UdHYa?usp=drive_link

Data Generation & Fine-Tuning Workflow

1. **Stage 1 – Scene Description Extraction**
   `dataset_generater/make_dataset_get_desc.py`
   `./datasets/descriptions/` containing: *{id, image_path, ocr_text, caption}*.
2. **Stage 2 – Augmented Prompt Synthesis**
   `third_party/make_dataset_with_nunchaku/make_dataset_with_augmentation.py`
   Invokes the *Nunchaku* augmentation engine to expand each record with synthetic corruptions (blur, noise, JPEG artifacts) and with diversity-enhanced textual prompts. The output is a paired folder structure: `./datasets/aug/{hq, lq}`.
3. **Stage 3 – Negative/HQ Pairing**
   `dataset_generater/make_dataset_Neg_HQ.py`
   Generates explicit (LQ, HQ) pairs and the associated prompt metadata required by GLYPH-SR. Final training files are placed under `./datasets/final/`.
4. **Stage 4 – Fine-Tuning**
   `train_GLYPH_SR.py`

```
python3 train_GLYPH_SR.py \
        --data_root ./datasets/ \
        --cfg       GLYPH-SR/model_configs/model_config.yaml
```

Inference Workflow

1. **Create the checkpoint directory.**
   Download every model file from the *Pre-trained Checkpoints* link and place them in a newly created folder named `CKPT_PTH` at the project root.
2. **Patch all path references.**
   Edit the three files listed below so that each points to the new directory, e.g. `CKPT_PTH/<checkpoint_name>.pth`:
   - `GLYPH-SR/model_configs/model_config.yaml`
   - `GLYPH-SR/run_GLYPH`$_S R$*.py*
   - `GLYPH-SR/CKPT_PTH.py`
3. **Run command.**
   Verify correct loading by launching a single-image run:

```
python3 run_GLYPH_SR.py --img_path ./image.jpg
```

Successful execution confirms that all checkpoints are discovered and that GLYPH-SR is ready for inference.

B.2 SETUP

All experiments were conducted on a workstation equipped with three NVIDIA RTX 6000 Ada GPUs (48 GB each), all utilized concurrently for training and inference, an Intel Xeon W9-3475X CPU (36 cores, 72 threads), and 256GB RAM. The system runs Ubuntu 24.04.2 LTS and uses a 3.7TB NVMe SSD for storage. The models were implemented in PyTorch 2.5.1 with CUDA 11.8.

B.2.1 EVALUATION DATASETS

ICDAR2017 (International Conference on Document Analysis and Recognition). The ICDAR2017 Robust Reading Challenge dataset consists of scene-text images designed to test text detection and recognition systems under real-world conditions. It includes both high- and low-quality images that exhibit various degradations such as blur, low resolution, and noise. This diversity makes it well-suited for fine-tuning vision-language models to enhance OCR robustness. In our pipeline, ICDAR2017 is used to fine-tune LLaVA-NeXT, enabling it to better handle degraded scene-text images and produce more accurate token-level guidance.

SCUT-CTW1500 (Curved Text in the Wild). SCUT-CTW1500 is a large-scale scene-text detection benchmark featuring 1,500 images with over 10,000 annotated curved text instances. The dataset includes a wide variety of natural scenes such as street views, signboards, and shop names, with text appearing in arbitrary orientations, lengths, and curvature. It is especially known for its high diversity in text shape and layout, which makes it well-suited for evaluating the robustness of text detection and SR models in processing long and curved text lines. SCUT-CTW1500 is widely used for benchmarking models designed to process irregular and multi-oriented scene-text under real-world conditions.

CUTE80 (Curve Text). CUTE80 is a compact yet challenging dataset containing 80 high-resolution images, specifically curated to evaluate curved text detection and recognition systems. The dataset features a range of naturally curved and perspective-distorted text instances embedded in complex backgrounds such as logos, signs, and posters. Despite its small size, CUTE80 is frequently used in literature to benchmark the generalization ability of text-focused models on non-horizontal and non-linear text structures. Its emphasis on difficult geometric deformations makes it a useful supplement to larger datasets for testing text-specific visual models under challenging conditions.

SVT (Street View Text). SVT is a benchmark dataset collected from Google Street View, consisting of 647 images with approximately 2,000 annotated text instances. It features naturally occurring scene-text with various distortions, backgrounds, lighting conditions, and orientations. Despite its relatively small size, SVT is widely used in the literature for benchmarking the performance of OCR and text SR models under real-world conditions. Its challenging scenarios make it suitable for evaluating model generalization and robustness in unconstrained environments.

B.2.2 PRE-TRAINED MODELS

LLaVA-NeXT. We employ **LLaVA-NeXT** Liu et al. (2024) as the vision–language front-end that extracts semantic context from low-resolution inputs. LLaVA-NeXT couples a CLIP-ViT visual encoder with a 7-B parameter LLM and is instruction-tuned on a large multimodal corpus, yielding state-of-the-art performance in fine-grained grounding, captioning, and region-level reasoning. Within our pipeline it automatically produces (i) image-level captions (*IMG prompts*) and (ii) spatially aligned OCR strings (*OCR prompts*); both streams are fed as high-level conditions to the diffusion backbone.

JuggernautXL (SDXL-based). For image generation we adopt **JuggernautXL**, a publicly released checkpoint built on *SDXL-base 1.0* and further fine-tuned for improved sharpness and color fidelity. The underlying SDXL architecture is trained on billions of image–text pairs and natively supports 1024×1024 resolution.

B.2.3 KEY HYPER-PARAMETERS

- **Vision–Language Encoder.** A frozen LLaVA-NeXT produces 2 048-dimensional multi-modal embeddings that act as cross-attention keys; because the encoder is not fine-tuned, it adds zero trainable parameters.
- **First Stage (VAE).** A 256×256 auto-encoder (4 latent channels, $4\times$ down-sampling) maps RGB images to a $64 \times 64 \times 4$ latent grid.
- **Denoising and Sampling.** We use the standard 1 000-step DDPM schedule wrapped by RESTORE-EDM sampling (default: 50 inference steps, classifier-free guidance scale annealed from 7.5 to 4.0).

B.2.4 SYNTHETIC TRAINING DATA

To train the TS-ControlNet, we curate a purpose-built synthetic dataset with four mutually exclusive partitions: *Positive/High-Quality*, *Positive/Low-Quality*, *Negative/High-Quality*, and *Negative/Low-Quality*. Each split is created by selectively degrading either global content or localized glyph regions while keeping spatial layout and annotations intact. This design lets the network disentangle text-specific cues from general image priors.

"id": "/SVT_image_x4/00_18.jpg"

"OCR": "Days Inn & Suites"

"prompt": "The image depicts a street scene with a focus on a sign for a hotel named **Days Inn & Suites.** ….. The image has a casual, everyday quality to it, likely intended to show the location of the hotel for travelers or passersby."

"id": "/SVT_image_x4/00_19.jpg"

"OCR": "Comfort Inn"

"prompt": "The image shows a sign for a hotel or motel named **Comfort Inn.** The sign is rectangular with rounded corners and is mounted on a vertical pole. ….. The focus is on the sign, and the image is taken from a slightly lower angle, which makes the sign stand out against the sky."

Figure 8: Step 1: JSONL metadata—`id`, OCR text, and scene prompt—generated by LLAVA-NEXT.

Step 1: Prompt-Metadata Extraction. Using a pretrained LLAVA-NEXT encoder and YAML-defined prompt templates, we batch-process scene-text images and record three fields in `JSONL`: image `id`, OCR text, and a scene-level `prompt`. Figure 8 illustrates the resulting metadata, produced by `make_dataset_get_desc.py`.

Step 2: Stylistic Augmentation. We prepend each prompt with a style token (e.g., *sunset glow*, *cinematic bokeh*) via `make_dataset_with_augmentation.py`. The enriched prompts drive a Flux-based diffusion model equipped with ControlNet and LoRA modules to generate visually diverse high-quality samples (Fig. 9).

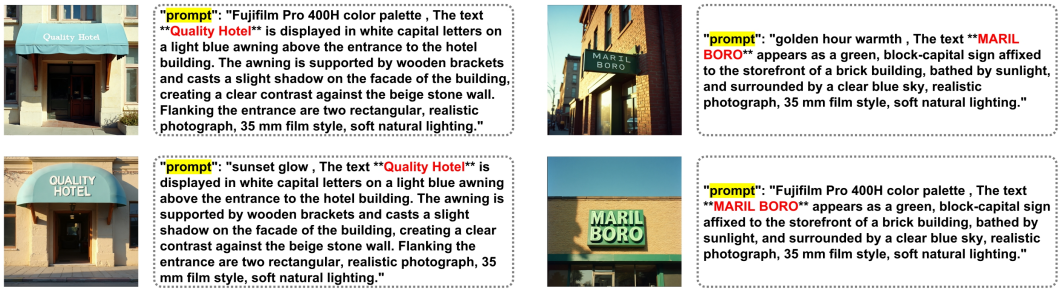

Figure 9: Step 2: Prompt augmentation with stylistic keywords to boost visual diversity.

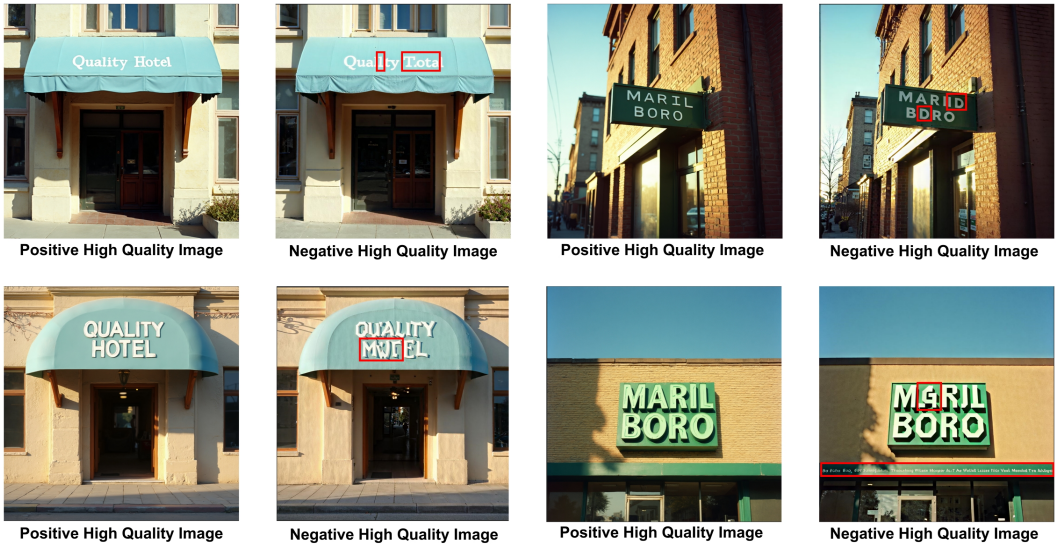

Figure 10: Step 3: Positive vs. intentionally corrupted (negative) high-quality pairs.

Step 3: Negative High-Quality Pairs. The `make_dataset_Neg_HQ.py` script corrupts text regions at the glyph level while leaving global detail untouched, yielding hard negative examples. Corruptions are verified with the SUPIR pipeline Yu et al. (2024b)(Fig. 10).

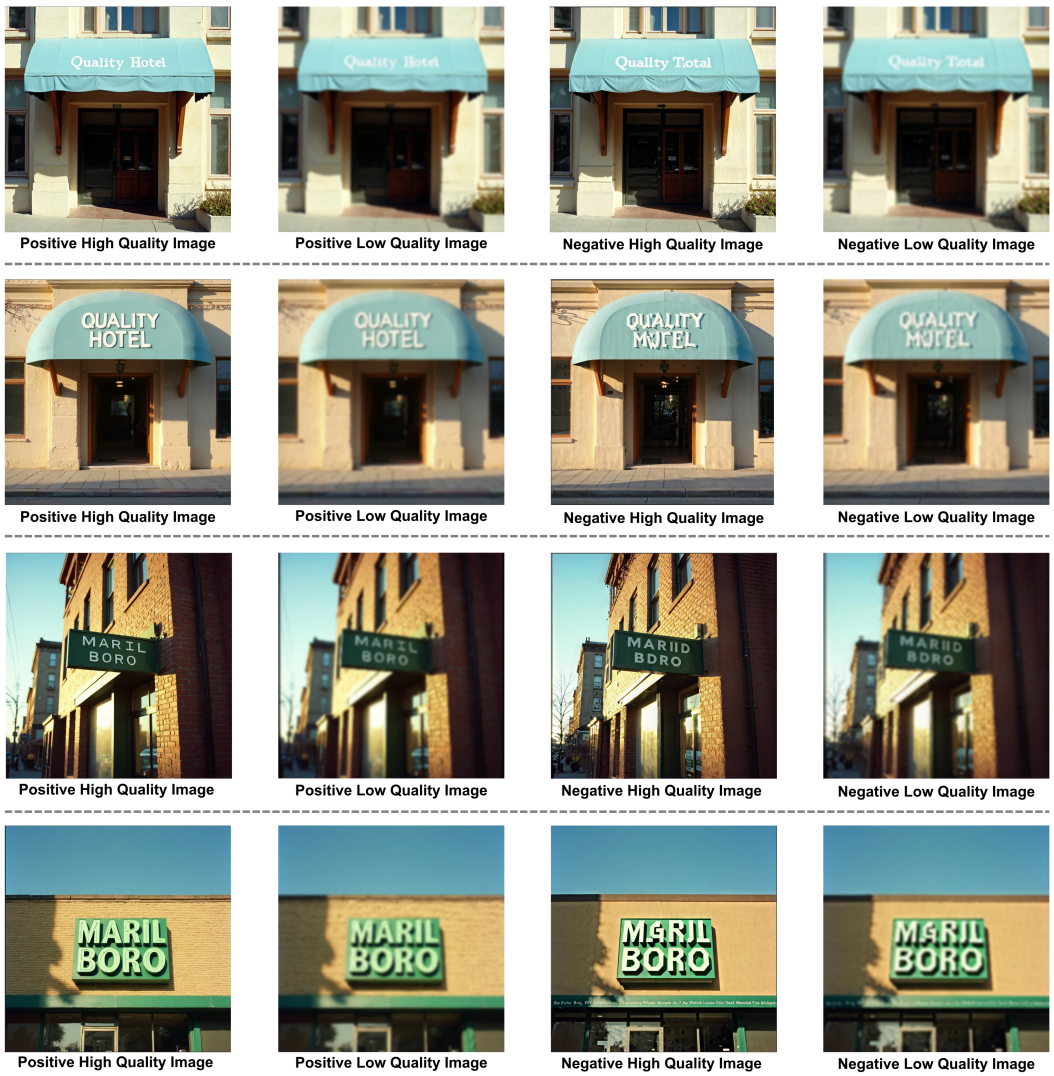

Figure 11: Step 4: Four synthetic subsets used for text-aware SR training.

Step 4: Final Dataset Assembly. All positive and negative images are merged into the four target splits shown in Fig. 11.

C EXPERIMENT RESULTS

C.1 COMPARE CHARACTER GENERATION TO OTHER MODELS.

Table 2: Quantitative comparison of OCR performance on images degraded by various factors and restored using six SR models, evaluated across three benchmark datasets and three OCR systems. Red and blue denote the best and second-best results, respectively.

	OpenOCR					GOT-OCR					LLaVA-NeXT				
	Precision	Recall	F_1 score	1-NED	Accuracy	Precision	Recall	F_1 score	1-NED	Accuracy	Precision	Recall	F_1 score	1-NED	Accuracy
SVT(x4)															
BSRGAN	57.03	51.19	53.96	28.04	36.95	69.63	50.68	58.66	31.29	41.50	**84.60**	57.55	68.50	15.82	52.09
DiffBIR	41.49	36.31	38.73	20.21	24.01	48.34	37.65	42.33	24.47	26.85	63.20	35.16	45.19	13.34	29.19
DiffTSR	39.55	12.81	19.35	14.27	10.71	51.76	14.39	22.51	15.97	12.68	78.98	17.94	29.23	5.49	17.12
InvSR	55.56	60.22	57.79	27.53	40.64	65.44	57.05	60.96	31.65	43.84	78.67	55.38	65.00	15.95	48.15
PiSA-SR	60.16	**66.79**	**63.30**	26.71	**46.31**	66.84	**63.70**	65.23	**33.74**	48.40	83.20	57.14	67.75	15.44	51.23
Real-ESRGAN	59.41	58.89	59.15	**30.16**	42.00	**75.05**	61.04	**67.32**	33.50	**50.74**	83.70	63.99	72.53	16.25	56.90
StableSR	**62.08**	57.83	59.88	**30.32**	42.73	**73.79**	56.13	63.76	**34.71**	46.80	**84.70**	**65.56**	**73.91**	**16.81**	**58.62**
SUPIR	58.16	58.67	58.41	20.17	41.26	64.54	59.48	61.90	26.81	44.83	74.54	53.28	62.14	15.86	45.07
GLYPH-SR (ours)	**61.33**	**75.14**	**67.54**	22.17	**50.99**	68.07	**75.79**	**71.72**	28.37	**55.91**	79.22	**68.07**	**73.22**	**19.49**	**57.76**
SCUT-CTW1500(x4)															
BSRGAN	46.41	16.80	24.67	29.86	14.07	56.71	13.54	21.86	23.70	12.27	78.96	22.56	35.10	17.25	21.28
DiffBIR	38.18	18.26	24.71	33.85	14.09	36.43	17.70	23.82	30.71	13.52	54.93	21.31	30.71	20.94	18.14
DiffTSR	45.86	12.60	19.77	25.83	10.97	50.84	9.48	15.98	18.64	8.69	72.82	14.14	23.69	11.30	13.43
InvSR	45.37	21.93	29.57	34.39	17.35	47.40	18.31	26.41	28.17	15.22	66.15	23.33	34.50	18.34	20.84
PiSA-SR	49.11	**30.27**	**37.46**	**40.32**	**23.04**	56.25	**24.50**	**34.14**	**33.47**	**20.58**	71.18	31.96	**44.11**	**23.23**	**28.30**
Real-ESRGAN	**52.95**	22.22	31.31	33.69	18.56	**59.50**	17.41	26.94	26.49	15.57	**79.94**	29.65	43.25	20.12	27.59
StableSR	**53.58**	16.77	25.55	30.02	14.64	**57.67**	12.06	19.95	22.18	11.08	**79.31**	**32.25**	**45.86**	21.07	**29.75**
SUPIR	39.95	11.84	18.26	25.73	10.05	45.16	10.93	17.61	21.40	9.65	62.60	15.13	24.37	14.32	13.87
GLYPH-SR (ours)	48.82	**31.46**	**38.26**	**37.75**	**23.66**	47.45	**30.27**	**36.96**	**36.09**	**22.67**	63.59	**32.37**	42.90	**25.86**	27.31
CUTE(x4)															
BSRGAN	68.84	**77.89**	**73.09**	**54.63**	**57.59**	69.44	**46.95**	56.02	**45.37**	38.91	92.54	76.86	83.97	39.00	72.37
DiffBIR	64.90	73.37	68.88	48.01	52.53	61.48	40.49	48.82	43.45	32.30	88.12	76.39	81.84	38.53	69.26
DiffTSR	64.94	57.65	61.08	51.95	43.97	67.80	36.53	47.48	**45.54**	31.13	92.59	61.22	73.71	30.66	58.37
InvSR	70.19	74.87	72.46	**53.54**	56.81	**72.79**	45.00	55.62	43.91	38.52	90.87	**79.41**	**84.75**	37.15	**73.54**
PiSA-SR	**71.36**	74.24	72.77	50.28	57.20	70.29	44.91	54.80	42.70	37.74	**93.30**	74.18	82.65	38.00	70.43
Real-ESRGAN	**71.43**	76.14	**73.71**	53.32	**58.37**	71.81	**49.77**	**58.79**	45.31	**41.63**	**93.03**	76.95	84.23	36.37	72.76
StableSR	69.71	74.74	72.14	51.76	56.42	**74.64**	46.40	**57.22**	42.36	**40.08**	89.66	77.12	82.92	38.02	70.82
SUPIR	68.78	73.06	70.85	49.43	54.86	63.38	43.90	51.87	42.38	35.02	89.05	76.17	82.11	**40.24**	69.65
GLYPH-SR (ours)	69.48	**77.08**	**73.09**	47.00	**57.59**	68.28	46.92	55.62	38.27	38.52	90.05	**80.51**	**85.01**	**39.78**	**73.93**
SVT(x8)															
BSRGAN	35.75	9.18	14.61	13.02	7.88	36.54	7.99	13.12	14.68	7.02	76.77	15.34	25.56	6.25	14.66
DiffBIR	25.00	12.54	16.70	16.56	9.11	29.23	13.58	18.55	18.51	10.22	44.16	14.93	22.32	10.21	12.56
DiffTSR	28.03	6.29	10.28	11.36	5.42	31.51	6.46	10.72	14.98	5.67	62.50	9.09	15.87	4.60	8.62
InvSR	29.34	12.08	17.12	**18.54**	9.36	37.80	14.68	21.15	**19.87**	11.82	50.00	13.73	21.54	8.20	12.07
PiSA-SR	36.11	11.57	17.53	14.53	9.61	47.84	16.06	24.05	19.83	13.67	**79.41**	24.77	37.76	7.72	23.28
Real-ESRGAN	34.50	11.93	17.73	16.17	9.73	48.20	15.35	23.29	19.45	13.18	76.68	19.30	30.83	7.14	18.23
StableSR	41.13	14.05	20.95	17.50	11.70	**50.45**	16.12	24.43	19.15	13.92	**79.43**	**29.71**	**43.24**	9.96	**27.59**
SUPIR	**42.82**	**27.66**	**33.61**	15.29	**20.20**	43.00	**30.90**	**35.96**	18.80	**21.92**	59.22	26.68	36.78	**11.28**	22.54
GLYPH-SR (ours)	**48.52**	**49.06**	**48.79**	**19.16**	**32.27**	**57.32**	**55.03**	**56.16**	**23.17**	**39.04**	69.57	**50.53**	**58.54**	**17.99**	**41.38**
SCUT-CTW1500(x8)															
BSRGAN	29.10	1.79	3.37	7.67	1.72	31.06	1.88	3.54	7.31	1.80	64.75	2.00	3.88	2.10	1.98
DiffBIR	15.66	2.81	4.76	17.18	2.44	11.46	3.28	5.10	**16.05**	2.62	21.26	2.60	4.64	**9.28**	2.37
DiffTSR	28.10	1.55	2.95	6.94	1.50	28.33	1.51	2.86	6.44	1.45	51.94	1.49	2.90	2.37	1.47
InvSR	21.15	1.10	2.09	7.13	1.06	18.66	1.15	2.17	7.17	1.10	55.45	1.24	2.43	1.78	1.23
PiSA-SR	25.50	**4.48**	**7.61**	**17.41**	**3.96**	29.21	**3.92**	**6.92**	13.26	**3.58**	50.45	**5.20**	**9.43**	6.82	**4.95**
Real-ESRGAN	**32.77**	2.72	5.02	9.82	2.57	**34.74**	3.07	5.64	9.91	2.90	**66.30**	4.11	7.74	3.81	4.02
StableSR	**39.90**	1.74	3.33	5.63	1.69	**40.55**	2.34	4.43	7.41	2.26	**71.37**	3.95	7.49	3.68	3.89
SUPIR	19.91	3.15	5.43	14.12	2.79	22.41	3.64	6.26	13.13	3.23	33.47	3.91	7.00	7.13	3.63
GLYPH-SR (ours)	22.61	**7.35**	**11.09**	**20.54**	**5.87**	25.24	**10.38**	**14.71**	**20.10**	**7.94**	34.12	**9.34**	**14.67**	**13.85**	**7.92**
CUTE(x8)															
BSRGAN	58.33	52.41	55.21	47.56	38.13	**68.42**	35.29	**46.57**	**42.81**	**30.35**	91.61	58.20	71.18	28.40	55.25
DiffBIR	**61.58**	57.67	**59.56**	45.10	**42.41**	58.73	36.10	44.71	38.97	28.79	88.61	58.58	70.53	30.10	54.47
DiffTSR	60.76	49.23	54.39	48.20	37.35	62.16	32.09	42.33	41.04	26.85	86.23	50.00	63.30	27.95	46.30
InvSR	55.80	57.06	56.42	47.28	39.30	60.98	35.89	45.18	39.50	29.18	87.43	61.86	72.46	**35.41**	56.81
PiSA-SR	58.23	48.17	52.72	**51.39**	35.80	61.61	32.24	42.33	41.76	26.85	**92.26**	**63.52**	**75.24**	30.23	**60.31**
Real-ESRGAN	60.67	57.75	59.18	50.53	42.02	**70.00**	**38.01**	**49.27**	**42.81**	**32.68**	**93.25**	61.79	**74.33**	31.11	**59.14**
StableSR	60.06	55.73	57.81	**51.68**	40.66	61.22	35.80	45.18	**43.35**	29.18	88.79	63.24	73.87	32.52	58.56
SUPIR	57.69	**58.33**	58.01	43.46	40.86	59.83	33.33	42.81	35.98	27.24	82.25	61.23	70.20	**35.16**	54.09
GLYPH-SR (ours)	**63.49**	**63.83**	**63.66**	42.40	**46.69**	58.91	**37.25**	45.65	36.80	29.57	83.80	**65.79**	73.71	35.12	58.37

We compare our model's character generation ability against standard OCR models across difficulty levels. The results in Table 2 show significant improvements, especially under hard conditions. For evaluation, LLaVA-NeXT and our model were prompted using the following instructions: *"Please perform OCR on this image."* Additionally, both predicted and ground truth texts were normalized by removing non-alphabetic characters and ignoring case sensitivity before computing the metrics.

Table 3: Quantitative comparison of SR models on three scene-text datasets (SVT, SCUT-CTW1500, CUTE80) at $\times 4$ and $\times 8$ upscaling factors. Metrics include distortion-based (PSNR, SSIM, LPIPS↓) and perceptual quality scores (MANIQA, CLIP-IQA, MUSIQ). Red and blue denote the best and second-best results, respectively.

Dataset	SR model	PSNR	SSIM	LPIPS↓	MANIQA	CLIP-IQA	MUSIQ
SVT(x4)	BSRGAN	28.09	83.16	35.34	38.16	39.63	66.25
	DiffBIR	21.96	63.94	43.55	**47.82**	**58.66**	**71.18**
	DiffTSR	26.06	78.42	44.95	21.34	27.69	46.24
	InvSR	24.78	76.58	38.61	46.78	57.30	70.81
	PiSA-SR	26.58	82.04	34.13	37.41	44.30	61.87
	Real-ESRGAN	**29.67**	**88.58**	**30.68**	31.16	28.58	51.14
	StableSR	**30.54**	**87.00**	**33.73**	24.75	32.18	24.44
	SUPIR	22.76	67.15	45.14	42.36	48.42	67.55
	GLYPH-SR (ours)	22.89	67.19	42.20	**47.75**	**59.40**	**70.99**
SCUT-CTW1500(x4)	BSRGAN	**20.22**	**64.59**	32.12	51.41	47.44	67.52
	DiffBIR	17.91	56.34	36.20	**62.37**	**61.90**	**71.19**
	DiffTSR	18.99	58.59	41.34	35.39	30.59	55.83
	InvSR	18.32	60.71	**32.99**	57.75	55.94	69.25
	PiSA-SR	20.07	63.99	**31.18**	56.31	53.05	68.19
	Real-ESRGAN	**20.85**	**67.46**	36.81	40.81	43.43	52.66
	StableSR	19.24	55.45	49.03	31.04	43.61	24.92
	SUPIR	13.61	32.98	52.15	57.35	51.68	66.96
	GLYPH-SR (ours)	18.19	54.67	37.15	**70.33**	**57.88**	**70.31**
CUTE80(x4)	BSRGAN	**27.35**	**79.76**	31.83	44.22	55.73	69.13
	DiffBIR	22.60	66.07	37.74	**51.04**	**72.64**	69.06
	DiffTSR	24.06	72.66	42.74	33.94	38.47	58.74
	InvSR	24.41	75.55	32.93	**50.30**	**67.78**	**70.66**
	PiSA-SR	25.83	77.41	**31.49**	45.82	61.81	66.18
	Real-ESRGAN	**28.14**	**82.30**	32.01	38.20	48.71	60.65
	StableSR	26.23	79.51	**30.45**	36.26	49.74	60.09
	SUPIR	22.42	66.20	39.33	47.50	62.62	68.26
	GLYPH-SR (ours)	23.03	69.54	37.03	49.77	65.93	**69.96**
SVT(x8)	BSRGAN	25.13	73.71	45.64	37.14	37.58	62.83
	DiffBIR	22.89	65.20	50.07	**45.54**	**53.20**	64.11
	DiffTSR	24.45	76.19	46.32	21.39	26.39	43.96
	InvSR	22.82	71.34	**41.84**	32.51	50.83	51.69
	PiSA-SR	**26.12**	77.64	50.83	34.02	18.39	30.24
	Real-ESRGAN	25.69	**80.28**	**41.92**	28.38	17.86	43.01
	StableSR	**26.38**	**78.15**	50.20	23.16	23.38	16.22
	SUPIR	21.23	59.08	51.46	40.17	45.06	**65.20**
	GLYPH-SR (ours)	21.77	61.36	47.85	**47.40**	**56.78**	**69.93**
SCUT-CTW1500(x8)	BSRGAN	**17.32**	**48.50**	47.86	46.21	37.83	**66.05**
	DiffBIR	15.78	43.47	**50.05**	54.75	**49.89**	63.16
	DiffTSR	14.83	40.25	54.50	35.49	31.88	50.43
	InvSR	11.81	30.68	65.88	29.65	29.62	40.29
	PiSA-SR	17.22	47.63	**48.90**	41.77	36.75	58.95
	Real-ESRGAN	**17.65**	**52.34**	52.14	28.37	20.95	39.99
	StableSR	17.00	43.50	66.02	20.93	20.92	16.62
	SUPIR	12.63	26.51	58.63	**55.46**	47.02	**65.55**
	GLYPH-SR (ours)	16.27	41.31	52.58	**61.94**	**48.21**	63.43
CUTE80(x8)	BSRGAN	**23.84**	**72.55**	**39.14**	42.07	54.31	**67.33**
	DiffBIR	22.77	65.36	41.79	**47.53**	62.09	64.62
	DiffTSR	22.67	70.41	42.80	33.55	42.95	57.47
	InvSR	21.83	70.76	**38.05**	37.66	**62.43**	57.69
	PiSA-SR	23.36	70.52	47.71	30.71	30.80	45.16
	Real-ESRGAN	**24.01**	**75.58**	39.60	35.17	36.46	56.55
	StableSR	7.94	35.66	79.75	26.00	40.42	34.48
	SUPIR	20.64	61.31	43.76	46.38	61.67	67.04
	GLYPH-SR (ours)	21.19	65.15	42.31	**47.75**	**65.85**	**68.85**

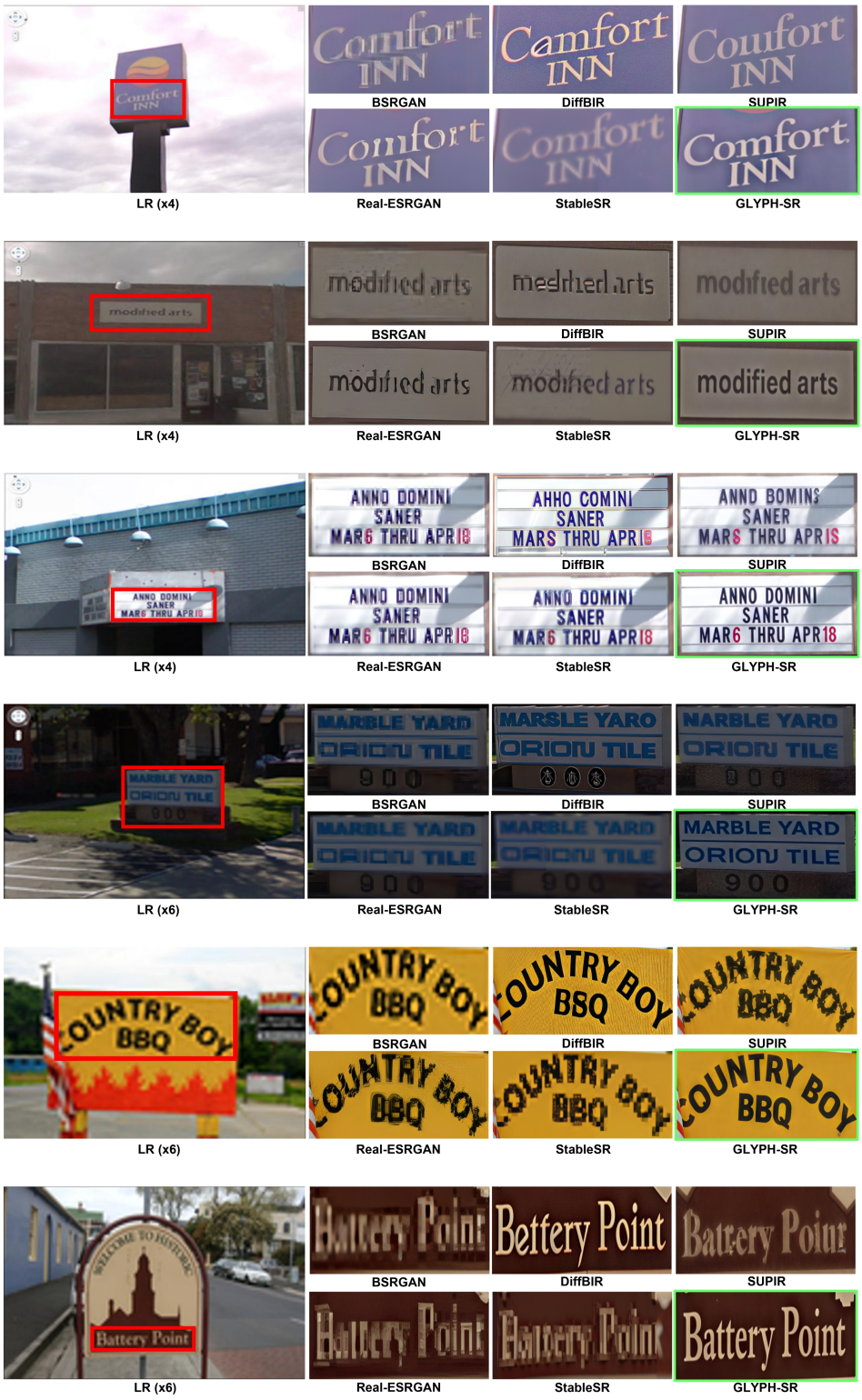
BSRGAN
DiffBIR
SUPIR
LR (x4)
Real-ESRGAN
StableSR
GLYPH-SR
BSRGAN
DiffBIR
SUPIR
LR (x4)
Real-ESRGAN
StableSR
GLYPH-SR
BSRGAN
DiffBIR
SUPIR
LR (x4)
Real-ESRGAN
StableSR
GLYPH-SR
BSRGAN
DiffBIR
SUPIR
LR (x6)
Real-ESRGAN
StableSR
GLYPH-SR
BSRGAN
DiffBIR
SUPIR
LR (x6)
Real-ESRGAN
StableSR
GLYPH-SR
BSRGAN
DiffBIR
SUPIR
LR (x6)
Real-ESRGAN
StableSR
GLYPH-SR

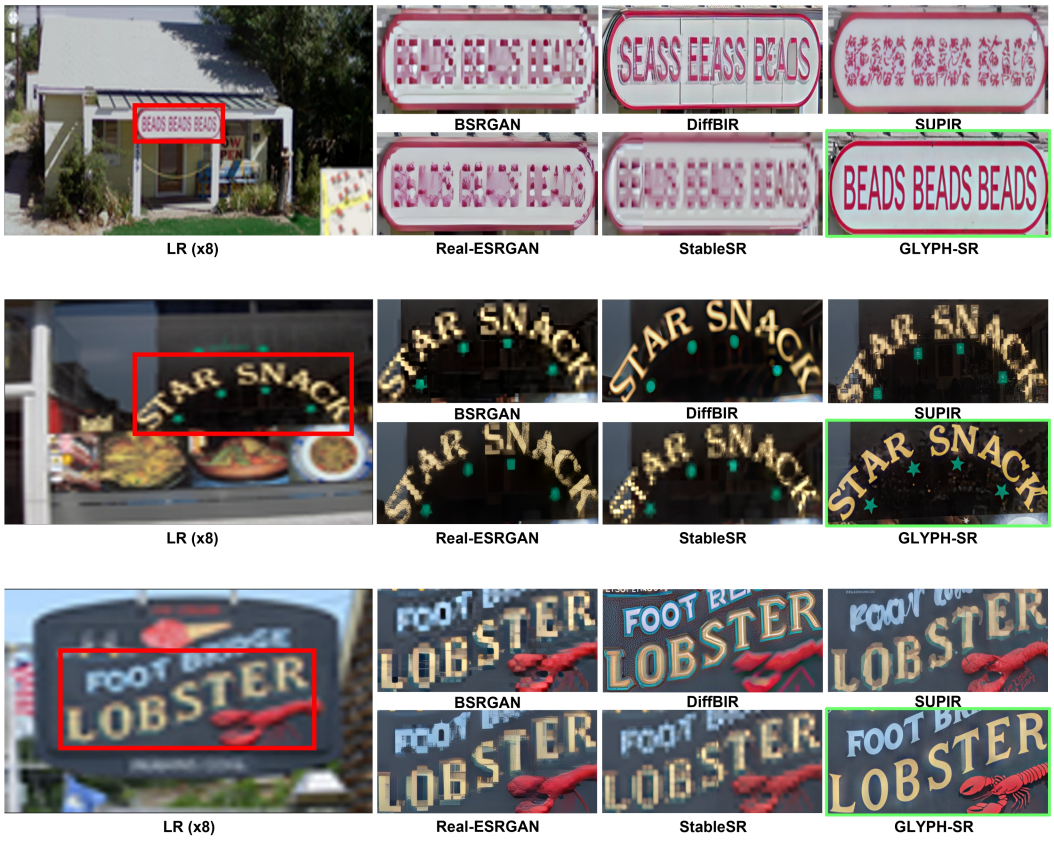

Figure 12: Qualitative comparison of scene-text SR under various degradation scales ($\times 4$, $\times 6$, $\times 8$). While prior methods often blur or hallucinate characters, **GLYPH-SR** accurately restores readable, coherent text. Zoom in for detail.

Figure 13: Qualitative comparison of text-centric SR results at $\times 4$, $\times 8$ and $\times 16$ scales.

Fig. 13 provides a qualitative comparison between GLYPH-SR and baselines at magnification factors of $\times 4$, $\times 8$, and an extreme $\times 16$. GLYPH-SR continuously reconstructs glyph outlines, stroke widths, and kerning while remaining true to the underlying truth, while harmonizing color and brightness with the surrounding background area. This visual evidence corroborates the quantitative gap observed in

Table 1: models that optimize solely for perceptual metrics (e.g. DiffBIR, Real-ESRGAN) or for edge contrast fall short on OCR fidelity once the scale factor exceeds $\times 8$. GLYPH-SR achieves coherent integration of text and imagery even under $\times 16$ SR.

C.2 Ablation study on ping-pong schedule

Table 4 presents results for the CUTE80 benchmark at x4 and x8 scales under two evaluation protocols. The binary strategy yields higher CLIP-IQA and MUSIQ scores—reflecting superior perceptual quality—while simultaneously boosting the OCR F_1 score (LLaVA-NeXT), supporting its effectiveness at balancing text readability and image fidelity.

Table 4: Ablation on the scheduler policy evaluated on the CUTE80 dataset.

(a) CUTE80 (LR $\times$ 4)

Scheduler Policy	MANIQA	CLIP-IQA	MUSIQ	OCR F_1
Binary ping–pong	49.77	65.93	69.96	**85.01**
Mixing ($\lambda_t = 0.1$)	**49.95**	**70.64**	**70.67**	81.57
Mixing ($\lambda_t = 0.3$)	49.04	69.56	69.75	83.18
Mixing ($\lambda_t = 0.5$)	47.57	65.47	68.95	84.23
Mixing ($\lambda_t = 0.7$)	47.86	68.91	68.83	81.84
Mixing ($\lambda_t = 0.9$)	48.85	69.11	69.13	82.65

(b) CUTE80 (LR $\times$ 8)

Scheduler Policy	MANIQA	CLIP-IQA	MUSIQ	OCR F_1
Binary ping–pong	47.75	65.85	68.85	**73.71**
Mixing ($\lambda_t = 0.1$)	**48.89**	67.65	**69.56**	66.49
Mixing ($\lambda_t = 0.3$)	47.44	**68.31**	68.86	69.87
Mixing ($\lambda_t = 0.5$)	46.57	64.07	67.35	73.40
Mixing ($\lambda_t = 0.7$)	45.80	67.98	67.19	66.84
Mixing ($\lambda_t = 0.9$)	45.58	67.66	67.18	68.88

C.3 Sensitivity to Upstream VLM/OCR Errors

We assess how errors in upstream text guidance (OCR/VLM) propagate to GLYPH–SR. Because our method deliberately conditions on tokenlevel strings and locations, corrupted guidance could degrade both readability and overall perceptual quality. We simulate three error modes and measure their impact on OCR and IQA metrics.

1. **Random Character Corruption:** Replace $n\% \in \{30, 50, 90\}$ of characters in the OCR string with uniformly sampled alternatives (random noise).
2. **Plausible Character Swaps ("Swap"):** Systematically replace characters with visually confusable counterparts from a curated set (e.g., `O`↔`0`, `I`↔`1`, `T`↔`7`).
3. **Missed Detections ("Drop"):** Remove a portion of OCRrecognized characters to emulate detection/recognition failures.

Table 5 reports OpenOCR/GOTOCR F_1 and MANIQA/CLIPIQA. Parentheses show absolute changes w.r.t. the uncorrupted baseline.

Table 5: **Sensitivity to OCR/VLM guidance errors.** Values in parentheses are absolute deltas from the baseline (lower is worse).

Error rate / Type	OpenOCR F_1	GOT-OCR F_1	MANIQA	CLIP-IQA
Baseline	48.82	38.36	62.01	79.69
30%	38.36 (-10.46)	28.67 (-9.69)	45.87 (-16.14)	63.65 (-16.04)
50%	32.03 (-16.79)	26.35 (-12.01)	45.39 (-16.62)	64.88 (-14.81)
90%	27.52 (-21.30)	26.35 (-12.01)	45.61 (-16.40)	66.00 (-13.59)
Swap	39.88 (-8.94)	33.12 (-5.24)	45.81 (-16.20)	66.00 (-13.69)
Drop	41.85 (-6.97)	32.03 (-6.33)	44.82 (-17.19)	65.30 (-14.39)

All error modes substantially hurt both axes: readability (*OpenOCR/GOTOCR* F_1) and perceived image quality (MANIQA/CLIPIQA). Even moderate noise (50%) reduces OpenOCR F_1 by 16.79 pp and MANIQA by 16.62 points. Plausible swaps and missed detections also trigger large drops, indicating that *quantity* (how many tokens are wrong), *nature* (plausible vs. random), and *absence* (drops) all impair glyph integrity and global appearance. This validates our design choice to use a strong, LRaware OCR/VLM and to treat guidance quality as a firstorder factor in textaware SR.

Figure 14: Failure cases where GLYPH-SR produces visually plausible SR outputs but incorrectly generates text in non-textual regions.

As illustrated in Fig. 14, GLYPH-SR can deliver visually plausible SR results yet still *hallucinates* glyphs in regions that were originally non-textual. This deficiency in text-region localization means the reconstructed text may be ambiguous, incomplete, or entirely spurious. Furthermore, when multiple words are present, the model tends to enhance only the most visually salient word and overlook the rest. These failure cases underline the necessity for finer-grained attention mechanisms and explicit supervision of glyph positions in future work.

C.4 Computational Footprint and Practical Efficiency

Setup. We benchmark inference on a $4\times$ SR task with 512×512 inputs. Times are mean $\pm$ std. over repeated runs. For methods that require a large VLM (SUPIR and GLYPH–SR), we used *two* NVIDIA A6000 GPUs; reported peak VRAM is the *sum* across both devices.

Table 6: **Compute comparison.** For VLMguided methods, #Params lists (*restoration*, *VLM*) in millions.

Method	#Params (M)	Inference (s / sample)	Peak VRAM (GB)
StableSR	153	79.98 ± 0.22	10.10
DiffBIR	385	53.14 ± 1.41	9.64
SUPIR	18, 152	25.25 ± 0.86	46.21
GLYPH–SR	13, 225	38.25 ± 1.28	43.56

GLYPH–SR trades extra parameters and memory for markedly better text fidelity: it couples a restoration backbone with a powerful OCR/VLM to reason about lowresolution text. This design improves accuracy but introduces a computational bottleneck. To mitigate the cost while keeping readability gains, we will pursue:

- **Lighter VLM Guidance.** Replace the current generalpurpose VLM with a compact, LRtextspecialized guider (or distill the guider), reducing parameter count and latency with minimal loss in guidance quality.

- **Inference Optimization ("Block Caching").** Cache and reuse guidance features that repeat across diffusion steps/tiles (e.g., projected text embeddings and crossattention KV maps), skipping redundant compute and lowering endtoend runtime.

These directions aim to preserve GLYPH–SR's strengths ("looks right *and* reads right") while improving deployability under realistic compute budgets.

Trainable parameters. Although the full model size is large due to the VLM, our *fine-tuning* recipe is lightweight. We freeze the diffusion backbone and update only two components:

1. **TS-ControlNet branch** (≈54.8M parameters) that handles text-guidance fusion.
2. **VLM LoRA adapter** (≈5.9M parameters) with low rank (r=8), `lora_alpha` of 32, and dropout of 0.05.

To minimize memory further, the large *frozen* VLM is loaded in 4-bit quantization (`nf4` with double quantization via BitsAndBytes).

Table 7: **Trainable parameter counts** (millions). Despite using a VLM, GLYPH–SR keeps *trainable* parameters modest via freezing and LoRA.

Metric	GLYPH-SR	PiSA-SR	SeeSR	StableSR	DiffBIR	SUPIR	DiffTSR
Trainable (M)	**60.7**	0.38	489.04	152.67	378.95	3865.64	55.31

Inference latency. The OCR/VLM guider is the main overhead driver. Out of a total per-image latency of 38.25 ± 1.28 seconds (Sec. C.4), the VLM component accounts for ≈ 8.46 seconds. Notably, while integrating the VLM increases total parameter *count*, the latency impact is not proportional. In practice, we retain training practicality with only 60.7M trainable parameters and observe that the rise in inference time is moderate relative to the parameter growth, yielding a favorable trade-off between accuracy (readability and IQA) and compute.

Implication. These results align with our compute study (Table 6): GLYPH–SR deliberately expends parameters on guidance quality to secure text fidelity, yet its fine-tuning footprint remains compact and deployable. Further efficiency gains are compatible with our design (e.g., lighter LR-text guiders and block caching for reusable guidance features).

REFERENCES FOR APPENDIX

[12] Sidi Yang, Tianhe Wu, Shuwei Shi, Shanshan Lao, Yuan Gong, Mingdeng Cao, Jiahao Wang, and Yujiu Yang. Maniqa: Multi-dimension attention network for no-reference image quality assessment. In Proceedings of the IEEE/CVF Conference on Computer Vision and Pattern Recognition Workshops (CVPRW), pages 2286–2295, 2022.

[13] Jianyi Wang, Kelvin CK Chan, and Chen Change Loy. Exploring clip for assessing the look and feel of images. In AAAI, 2023.

[14] Jun Ke, Guy Hacohen, Phillip Isola, William T. Freeman, Michael Rubinstein, and Eli Shechtman. Musiq: Multi-scale image quality assessment. In Proceedings of the IEEE/CVF International Conference on Computer Vision (ICCV), pages 8827–8837, 2021.

[18] Haotian Liu, Chunyuan Li, Yuheng Li, Bo Li, Yuanhan Zhang, Sheng Shen, and Yong Jae Lee. Llava-next: Improved reasoning, ocr, and world knowledge, January 2024.

[20] Fanghua Yu, Jinjin Gu, Zheyuan Li, Jinfan Hu, Xiangtao Kong, Xintao Wang, Jingwen He, Yu Qiao, and Chao Dong. Scaling up to excellence: Practicing model scaling for photo-realistic image restoration in the wild. In Proceedings of the IEEE/CVF Conference on Computer Vision and Pattern Recognition, pages 25669–25680, 2024.

[21] Richard Zhang, Phillip Isola, Alexei A. Efros, Eli Shechtman, and Oliver Wang. The unreasonable effectiveness of deep features as a perceptual metric. In Proceedings of the IEEE Conference on Computer Vision and Pattern Recognition (CVPR), June 2018.

[22] Yochai Blau and Tomer Michaeli. The perception-distortion tradeoff. In Proceedings of the IEEE Conference on Computer Vision and Pattern Recognition (CVPR), June 2018.

[23] Gu Jinjin, Cai Haoming, Chen Haoyu, Ye Xiaoxing, Jimmy S Ren, and Dong Chao. Pipal: a large-scale image quality assessment dataset for perceptual image restoration. In Computer Vision–ECCV 2020: 16th European Conference, Glasgow, UK, August 23–28, 2020, Proceedings, Part XI 16, pages 633–651. Springer, 2020.

[24] Jinjin Gu, Haoming Cai, Chao Dong, Jimmy S. Ren, Radu Timofte, Yuan Gong, Shanshan Lao, Shuwei Shi, Jiahao Wang, Sidi Yang, Tianhe Wu, Weihao Xia, Yujiu Yang, Mingdeng Cao, Cong Heng, Lingzhi Fu, Rongyu Zhang, Yusheng Zhang, Hao Wang, Hongjian Song, Jing Wang, Haotian Fan, Xiaoxia Hou, Ming Sun, Mading Li, Kai Zhao, Kun Yuan, Zishang Kong, Mingda Wu, Chuanchuan Zheng, Marcos V. Conde, Maxime Burchi, Longtao Feng, Tao Zhang, Yang Li, Jingwen Xu, Haiqiang Wang, Yiting Liao, Junlin Li, Kele Xu, Tao Sun, Yunsheng Xiong, Abhisek Keshari, Komal, Sadbhawana Thakur, Vinit Jakhetiya, Badri N Subudhi, Hao-Hsiang Yang, Hua-En Chang, Zhi-Kai Huang, Wei-Ting Chen, Sy-Yen Kuo, Saikat Dutta, Sourya Dipta Das, Nisarg A. Shah, and Anil Kumar Tiwari. Ntire 2022 challenge on perceptual image quality assessment. In Proceedings of the IEEE/CVF Conference on Computer Vision and Pattern Recognition (CVPR) Workshops, pages 951–967, June 2022.

[25] Fanghua Yu, Jinjin Gu, Zheyuan Li, Jinfan Hu, Xiangtao Kong, Xintao Wang, Jingwen He, Yu Qiao, and Chao Dong. Scaling up to excellence: Practicing model scaling for photo-realistic image restoration in the wild. In Proceedings of the IEEE/CVF Conference on Computer Vision and Pattern Recognition (CVPR), pages 25669–25680, June 2024.